The Generalised Fully Lagrangian Approach for Polydisperse Sprays. Implementation of a two-way coupling model in OpenFOAM.

Chris Stafford, Oyuna Rybdylova*
Advanced Engineering Centre, School of Architecture, Technology and Engineering,
University of Brighton, Brighton, BN2 4GJ, UK
*Corresponding author: o.rybdylova@brighton.ac.uk

Abstract
The generalised fully Lagrangian approach (gFLA) is an extension of the original fully Lagrangian approach (FLA, also known as Osiptsov's method), which aims to model polydisperse evaporating sprays. The FLA is known for its advantages in application to particle-laden flows. This approach makes it possible to capture detailed structures in the particulate clouds, including where particle trajectories cross and particles collect in narrow regions. It has proven to be an efficient approach for dilute mixtures and recently it was applied to polydisperse evaporating sprays. This work is focused on two-way coupling, where the effect of droplets on the carrier phase is taken into account. Kernel regression is used for interpolation of Lagrangian data in calculation of momentum and mass exchange terms. The implementation has been validated against the existing two-way coupling procedures within OpenFOAM.

Introduction
Gas-droplet flows are widely observed in engineering and environmental settings [1], for example aerosols generated when coughing and sneezing [2], and in applications, for example aerosol drug delivery [3] and during fuel injection in internal combustion engines [4]. The fundamental physics involved is essentially the interaction between a dispersed phase of droplets and a carrier phase, that includes not only momentum exchange, but also phase change in some applications. To accurately capture the effect of droplets on the carrier phase, it is essential to have a rigorous calculation of momentum and mass exchange terms, especially in areas of droplet accumulation.
This paper follows the chain of works on development of the fully Lagrangian approach for dilute mixtures. In such flows, the admixture forms high concentration regions with folds (local zones of crossing particle/droplet trajectories, hereafter referred to as droplets) and caustics. At the edge of a local region of crossing particle trajectories (caustics), the particle number density has a singularity. This is a well-known feature of the mathematical model of the collisionless continuum of point particles (see details in [8], where typical examples of flows with singularities in the particle number density field were analysed). It was shown that for an integrable singularity of particle number density, at the singular points the mean distance between the particles remains finite and the model of collisionless particles remains valid. The fully Lagrangian approach (FLA) has become known for its potential to capture such complex structures in gas-droplet flows while providing number density values in Lagrangian droplet positions [5, 6]. Moreover, it has been demonstrated that the FLA is an efficient method for calculating droplet distributions in comparison to other Lagrangian approaches [6]. In [7], a generalised FLA (gFLA) was applied to polydisperse evaporating sprays. It was shown that while the gFLA maintained advantages of the original FLA, there was a need to develop a robust method for interpolation of Lagrangian data to a Eulerian mesh. This was achieved by implementation of kernel regression [9], which takes advantage of the continuum description provided by the FLA to realize the potential computational economy of the approach through an efficient statistical procedure. The kernel regression retains the detail of complex structures in droplet clouds, caustics and voids, by sizing the kernel domain of influence using the information about the local droplet deformation field provided by the FLA or gFLA.
This paper is concerned with the next step in the development of the FLA/gFLA; implementation of two-way coupling. In our approach, the momentum and mass source terms, which describe the effect of droplets on the carrier phase flow, are calculated using kernel regression [9]. The paper is arranged as follows: mathematical models of the gas-droplet flow are described in Section 1; results of the application of the new OpenFOAM solver to the analysis of a two-phase flow around a cylinder are presented and discussed in Section 2; and the main results of the paper are summarised in Section 3.

Mathematical models of the carrier and dispersed phases
Note that in the paper we use non-dimensionalised equations and expressions, where the flow parameters are scaled using characteristic length and velocity values, L and U. The values of L and U are chosen for specific flow scenarios and are explained in Section 2.

Carrier phase
The carrier phase is modelled as an incompressible or compressible viscous flow of fluid described by the mass continuity and Navier–Stokes equations. In the case of an incompressible flow these equations are presented as

$$\nabla \cdot \mathbf{u} = 0, \tag{1a}$$

$$\frac{\partial \mathbf{u}}{\partial t} + (\mathbf{u} \cdot \nabla)\mathbf{u} = -\nabla p + \frac{1}{Re}\nabla^2 \mathbf{u} + S_{\text{Mom}}, \tag{1b}$$

where $\mathbf{u}$ is the gas velocity, p is the static pressure, and S_{Mom} is the momentum exchange term from the droplet phase. The flow Reynolds number is

$$Re = \frac{\rho L U}{\mu},$$

where L and U are characteristic length and velocity scales, μ is the fluid dynamic viscosity, and ρ is the carrier phase density. Since the focus of the work is on sprays, hereafter, the carrier phase considered is gaseous.
The passive scalar equation describing droplet liquid vapour diffusion and advection is taken in the following form

$$\frac{\partial c}{\partial t} + \nabla \cdot (D \nabla c) + \nabla \cdot (\mathbf{u} c) = S_{\text{Mass}}, \tag{2}$$

where c is the droplet vapour concentration, D is the vapour-carrier gas diffusion coefficient, and S_{Mass} is the mass exchange term. The source terms S_{Mom} and S_{Mass} describe the effect of droplets on the carrier flow gas, and these terms will be described in the following section.

Physical models for droplets

Whilst the FLA/gFLA formulation (described in the section below) is applicable to general equations of motion and evaporation/condensation for particle and droplets modelled as point masses in a dilute suspension, we restrict our analysis to gas-droplet flows. Since the liquid density is much greater than the carrier flow gas density, buoyancy, added-mass, and Basset-Boussinesq forces can be ignored. Assuming low droplet Reynolds number enables us to model the droplet momentum using the Stokes drag law. For a simplified physical model of evaporation, all heat at the droplet surface is taken to be spent on evaporation, then the droplet evaporation rate only depends on the droplet radius. Under these conditions, the expressions for the force per unit of droplet mass and the droplet's evaporation rate take form:

$$\mathbf{f} = \frac{1}{St_0\, r^2} \left(\mathbf{u} - \mathbf{v}_d \right), \tag{3a}$$

$$\varphi = -\frac{\delta}{2r}, \tag{3b}$$

where St_0 is a reference droplet Stokes number corresponding to the initial modal droplet size, $\mathbf{u}$ is the carrier flow velocity, $\mathbf{v}_d$ is droplet velocity, $\mathbf{f}$ is the force per unit mass, φ is the rate of droplet radius change due to evaporation, and δ is the rate of change of the droplet surface area.

The generalised fully Lagrangian approach for droplet distribution calculations

The governing equations and corresponding initial conditions for droplet motion and evaporation are:

$$\ddot{\mathbf{x}}_d(t) = \mathbf{f}(\mathbf{x}_d(t), \mathbf{v}_d(t), r_d(t), t), \tag{4a}$$

$$\dot{r}_d(t) = \varphi(\mathbf{x}_d(t), \mathbf{v}_d(t), r_d(t), t), \tag{4b}$$

$$\mathbf{x}_d(t_0) = \mathbf{x}_0, \tag{4c}$$

$$\dot{\mathbf{x}}_d(t_0) = \mathbf{v}_0, \tag{4d}$$

$$r_d(t_0) = r_0, \tag{4e}$$

where $\mathbf{f}$ is the force per unit mass exerted on a droplet, which is usually a known function of the droplet size, droplet velocity, and other parameters; $\dot{r}_d = \varphi$ is the rate of droplet size change, which is usually a known function of the droplet size and thermodynamic parameters, and the subscript d denotes that parameters are described in a Lagrangian frame of reference along droplet trajectories.
According to the fully Lagrangian approach, the droplet cloud is represented as a continuum. The Lagrangian variables are the droplet initial position coordinates $\mathbf{x}_0$, which together with time t define the current droplet location. Extending the set of Lagrangian variables to include the initial size r_0 makes it possible to describe polydisperse and evaporating droplets [5, 7]. The droplet distribution function $p(\mathbf{x}_d, r_d, t)$ can be found from the Lagrangian form of the continuity equation

$$p(\mathbf{x}_d, r_d, t) = \frac{p(\mathbf{x}_0, r_0, t_0)}{|\det(\mathbf{J}(\mathbf{x}_0, r_0, t))|}, \tag{5}$$

where the Jacobian tensor $\mathbf{J}(\mathbf{x}_0, r_0, t)$ is defined by

$$\mathbf{J}(\mathbf{x}_0, r_0, t) = \begin{bmatrix} \mathbf{J}^{\mathbf{xx}} & \mathbf{J}^{\mathbf{x}r} \\ \mathbf{J}^{r\mathbf{x}} & J^{rr} \end{bmatrix} = \begin{bmatrix} \frac{\partial \mathbf{x}_d}{\partial \mathbf{x}_0} & \frac{\partial \mathbf{x}_d}{\partial r_0} \\ \frac{\partial r_d}{\partial \mathbf{x}_0} & \frac{\partial r_d}{\partial r_0} \end{bmatrix}. \tag{6}$$

The equations for the Jacobian components are obtained by taking partial derivatives of Eqs. (4) with respect to the

Lagrangian variables

$$\ddot{\mathbf{J}}^{\mathbf{xx}} = \frac{\partial \mathbf{f}_d}{\partial \mathbf{x}} \cdot \mathbf{J}^{\mathbf{xx}} + \frac{\partial \mathbf{f}_d}{\partial \mathbf{v}} \cdot \dot{\mathbf{J}}^{\mathbf{xx}} + \frac{\partial \mathbf{f}_d}{\partial r} \mathbf{J}^{r\mathbf{x}}, \tag{7a}$$

$$\ddot{\mathbf{J}}^{\mathbf{x}r} = \frac{\partial \mathbf{f}_d}{\partial \mathbf{x}} \cdot \mathbf{J}^{\mathbf{x}r} + \frac{\partial \mathbf{f}_d}{\partial \mathbf{v}} \cdot \dot{\mathbf{J}}^{\mathbf{x}r} + \frac{\partial \mathbf{f}_d}{\partial r} J^{rr}, \tag{7b}$$

$$\dot{\mathbf{J}}^{r\mathbf{x}} = \frac{\partial \varphi_d}{\partial \mathbf{x}} \cdot \mathbf{J}^{\mathbf{xx}} + \frac{\partial \varphi_d}{\partial \mathbf{v}} \cdot \dot{\mathbf{J}}^{\mathbf{xx}} + \frac{\partial \varphi_d}{\partial r} \mathbf{J}^{r\mathbf{x}}, \tag{7c}$$

$$\dot{J}^{rr} = \frac{\partial \varphi_d}{\partial \mathbf{x}} \cdot \mathbf{J}^{\mathbf{x}r} + \frac{\partial \varphi_d}{\partial \mathbf{v}} \cdot \dot{\mathbf{J}}^{\mathbf{x}r} + \frac{\partial \varphi_d}{\partial r} J^{rr}, \tag{7d}$$

$$\mathbf{J}^{\mathbf{xx}}(\mathbf{x}_0, r_0, t_0) = \mathbf{I}, \tag{7e}$$

$$\dot{\mathbf{J}}^{\mathbf{xx}}(\mathbf{x}_0, r_0, t_0) = \frac{\partial \mathbf{v}_0}{\partial \mathbf{x}_0}, \tag{7f}$$

$$\mathbf{J}^{\mathbf{x}r}(\mathbf{x}_0, r_0, t_0) = \mathbf{0}, \tag{7g}$$

$$\dot{\mathbf{J}}^{\mathbf{x}r}(\mathbf{x}_0, r_0, t_0) = \mathbf{0}, \tag{7h}$$

$$\mathbf{J}^{r\mathbf{x}}(\mathbf{x}_0, r_0, t_0) = \mathbf{0}, \tag{7i}$$

$$J^{rr}(\mathbf{x}_0, r_0, t_0) = 1, \tag{7j}$$

where $\mathbf{I}$ is the identity matrix. The initial conditions for the system (7) are found from the initial conditions associated with the governing equations (4).
In the case of monodisperse droplets (standard FLA), the probability density $p(\mathbf{x}_d, r_d, t)$ reduces to the number density $n(\mathbf{x}_d, t)$, which is a function of droplet position $\mathbf{x}_d$ only.
Returning to the momentum and mass exchange terms in equations (1b) and (2), these can be defined using the droplet distribution function as follows:

$$S_{\text{Mom}} = -\int_r p(\mathbf{x}_d, r_d, t) m(r) \dot{\mathbf{v}}_d \, dr, \tag{8a}$$

$$S_{\text{Mass}} = -\int_r p(\mathbf{x}_d, r_d, t) \dot{m}(r) \, dr, \tag{8b}$$

in which m is the mass of a droplet with radius r.

Kernel regression and its application to calculating phase exchange terms

The FLA described in the previous section is used to calculate the droplet parameters, droplet number density values in particular, along trajectories (in Lagrangian coordinates). This data then needs to be remapped onto an Eulerian field. In [9], it was proposed to use kernel regression for droplet data interpolation due to the flexibility of this approach. There is no limit on the minimal number of data points needed (one is sufficient), and it can be extended to the case of multivalued droplet parameter fields and polydisperse droplets. In our study, we consider the Nadaraya-Watson estimator [10]

$$p(\mathbf{x}, r, t) = \frac{\sum_{i=1}^{N} K_{\mathbf{H}}(\mathbf{x}, r, \mathbf{x}_d^i, r_d^i) \, p(\mathbf{x}_d^i, r_d^i, t)}{\sum_{j=1}^{N} K_{\mathbf{H}}(\mathbf{x}, r, \mathbf{x}_d^j, r_d^j)}, \tag{9}$$

where $p(\mathbf{x}_d^i, r_d^i, t)$ is the instantaneous probability density along the phase space trajectory $(\mathbf{x}_d^i, r_d^i)$ associated with the i^{th} droplet at time t as obtained from the gFLA, $p(\mathbf{x}, r, t)$ is the Eulerian probability density field, N is the number of droplets that contribute at the phase space point $(\mathbf{x}, r)$, and $K_{\mathbf{H}}(\mathbf{x}, r, \mathbf{x}_d^i, r_d^i)$ is the kernel. A multivariate Gaussian form is chosen in this work, and a corresponding kernel can be defined as

$$K_{\mathbf{H}}(\mathbf{x}, r, \mathbf{x}_d^i, r_d^i) = \frac{1}{\sqrt{\det(\mathbf{H})}} \exp\left[-\frac{1}{2} \begin{pmatrix} \mathbf{x} - \mathbf{x}_d^i \\ r - r_d^i \end{pmatrix}^{\top} \cdot \mathbf{H}^{-1} \cdot \begin{pmatrix} \mathbf{x} - \mathbf{x}_d^i \\ r - r_d^i \end{pmatrix} \right], \tag{10}$$

where $\mathbf{H}$ is the bandwidth matrix that contains information about the smoothing lengths in different directions, e.g. $\mathbf{H} = h^2\mathbf{I}$ corresponds to a spherical kernel with a smoothing length h. In the case of polydisperse droplets, which includes the behaviour of the droplet radius r_d, the bandwidth matrix $\mathbf{H}$ is defined as

$$\mathbf{H}(\mathbf{x}_0, r_0, t) = \begin{bmatrix} h_{\mathbf{x}0}^2 |J^{\mathbf{xx}}(\mathbf{x}_0, r_0, t)|^{2/n} \mathbf{I} & \mathbf{0} \\ \mathbf{0} & h_{r0}^2 |J^{rr}(\mathbf{x}_0, r_0, t)|^2 \end{bmatrix} \tag{11}$$

where $h_{\mathbf{x}0}$ and h_{r0} are the initial smoothing lengths in physical and radial space respectively, and n is the spatial dimensionality of the problem. This form of the bandwidth matrix takes into account information about local deformation in the droplet phase by including the Jacobian blocks.
In this study, it is assumed that the droplet liquid density remains the same, which makes the droplet mass calculations straightforward, where droplet mass depends only on its size. The droplet distribution function is reconstructed using equation (9). Note, however, that in the expressions for the source terms (8), it is required to calculate contributions to momentum and mass exchange from droplets of all the sizes weighted by the distribution function. Therefore, equation (9) is adapted for calculation of the integrands in (8); then the source terms are evaluated using the trapezoidal rule.

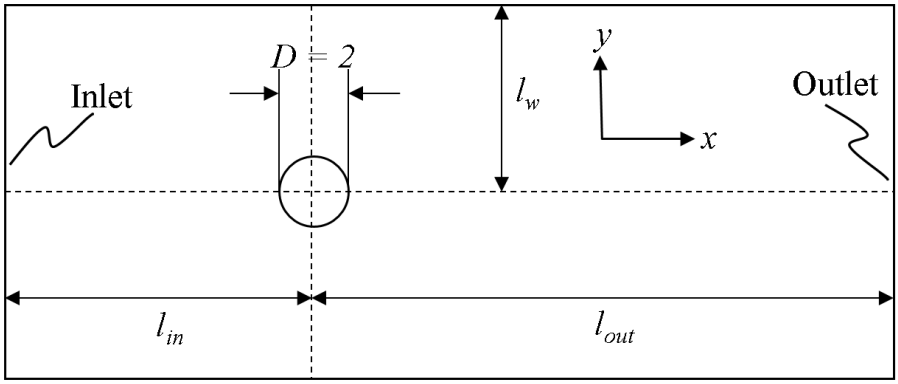

Figure 1. The 2D computational domain of the gas flow past the circular cross-section of a cylinder with a diameter of 2. l_{in}, l_{out} and l_w represent the distance from the centre of the cylinder to the inlet boundary on the left, the outlet boundary on the right and the periodic boundaries on the top and the bottom.

Results and discussion

The developed approach of combining the gFLA with kernel regression has been implemented in the open-source CFD code OpenFOAM as an additional library. In this section we discuss 2D steady-state and periodic gas-droplet flows around a cylinder with both monodisperse and polydisperse droplets. The gas (carrier phase) parameters are calculated using the OpenFOAM pimpleFoam solver, whereas the droplet parameters are reconstructed using the newly implemented library. For the purposes of verification of the implementation and testing the functionality, we limit our study to Stokes's drag law, neglecting other forces and assuming low droplet Reynolds numbers. As in Section 1, it is assumed that droplets evaporate into their own vapour and all heat at the droplet surface is spent on its evaporation. These assumptions lead to simplified expressions for the force $\mathbf{f}$ and evaporation rate φ used in equation (3). The above assumptions on physical models can be relaxed by replacing the expressions for $\mathbf{f}$ and φ by models corresponding to more realistic flow scenarios.

Fluid flow around a cylinder is a classical problem and is often used as a benchmark for computational fluid dynamics codes [11]. Depending on the flow Reynolds number, various flow regimes may be observed, including symmetric stationary flow with attached recirculation zones and periodic flows [12].

The flow domain and some notation used in the simulations is shown in Figure 1; $x \in [-l_{in}, l_{out}]$ and $y \in [-l_w, l_w]$, and the origin of the Cartesian coordinate system is located in the centre of the circle. The length and velocity scales are chosen to be the radius of the cylinder and the free-stream velocity. The Reynolds number values used in this paper are half of those in works where the diameter of the cylinder is used as the length scale, as in for example [12]. The values of l_{in}, l_{out} and l_w are set at 20, 30, and 20 respectively. See [7] for full details of the numerical setup, including assessment of the mesh and domain size.

The inlet velocity is normal to the inlet. The outlet velocity condition is set as zero-gradient. The inlet and outlet pressure are set as zero-gradient and a fixed value of zero, respectively. On the cross-section of the cylinder wall, there is a no-slip condition for the velocity and zero-gradient condition for pressure. The boundary conditions at the top and bottom edges of the computational domain are set as periodic.

Normally, in such a study of flow past a cylinder, the inlet velocity is fixed to be equal to the free-stream velocity in the far field. In this work, to model the case of a periodic flow, a transient perturbation was deliberately introduced at the inlet at an initial stage to trigger the onset of vortex shedding. It is inevitable that an asymmetric flow field corresponding to vortex shedding will develop in a computation with a symmetric configuration, providing that Re is sufficiently large and the computational time is sufficiently long. It is known that the asymmetry in simulations stems from truncation errors of computational models. Thus, improving the spatial and temporal resolution, which increases the accuracy, delays the start of vortex shedding. An asymmetrical longitudinal disturbance of the inlet velocity introduced at the initial stage was reported to significantly reduce the computational time for generating the periodic flow field [13]. The velocity at the inlet, $x = -l_{in}$, $y \in [-l_w, l_w]$, is defined as follows

$$\mathbf{u}(-l_{in}, y, t) = \begin{cases} (1 + ae^{-\zeta t}\sin(ky), 0) & \text{for } t \leq 10, \\ (1, 0) & \text{for } t > 10. \end{cases} \tag{12}$$

Here a and k are the amplitude and wave number of the disturbance, and ζ is the damping parameter. Their values are chosen as

$$a = 0.2, \quad k = \frac{\pi}{10}, \quad \zeta = 1. \tag{13}$$

As demonstrated in [13], these values have an effect on the length of the computational time taken to start generating the periodic flow, but not the flow pattern itself.

For the carrier phase, the pimpleFoam solver was configured as outlined in [14]. The computational mesh was constructed in such a way that its quality within the boundary layer around the cylinder could be defined explicitly.

The results of the FLA/gFLA simulations in the case of one-way coupling have been reported in [9]. In this paper, we focus on the implementation of two-way coupling, when accounting for the effect of droplets on the carrier phase in

both stationary and transient cases. Selected results are presented in Figures 2 – 5. In the first case, we consider a stationary flow around the cylinder, $Re = 20$. For calculation of the combined FLA and kernel regression procedure, 100 seed particles injected every 0.1 seconds were used. In the reference case, the particle parameters were calculated using the Cloud-In-Cell (CIC) method, which required 1000 seed particles injected every 0.01 seconds. Comparison of the results for the momentum exchange values is presented in Figures 2 and 3. The results obtained using the two methods are in good agreement. The calculations using the CIC method took 3040 CPU hours vs. 22 hours required for the FLA and kernel regression procedure.

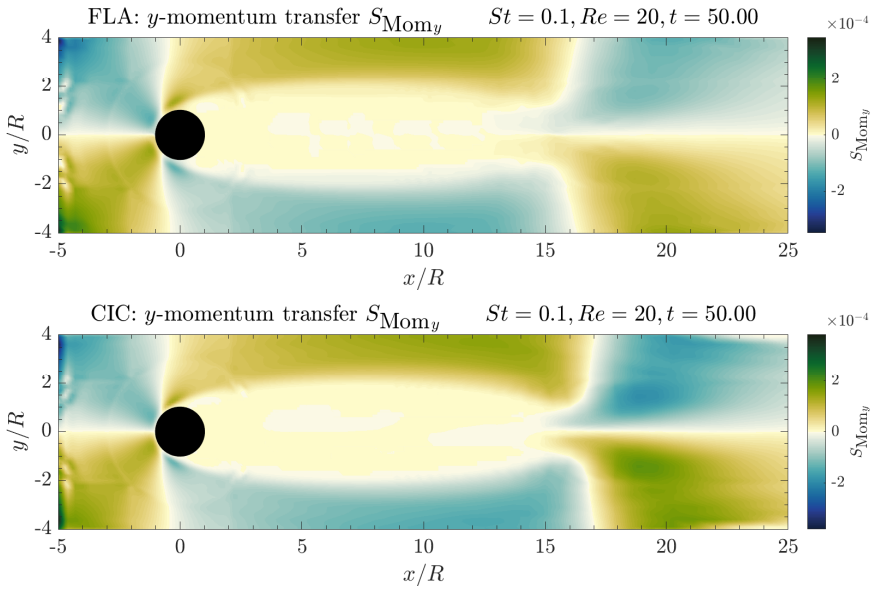

Figure 2. Distribution of the $y-$component of the momentum source term S_{Mom}, calculated using FLA + kernel regression (top) and CIC (bottom), $Re = 20$, $St = 0.1$.

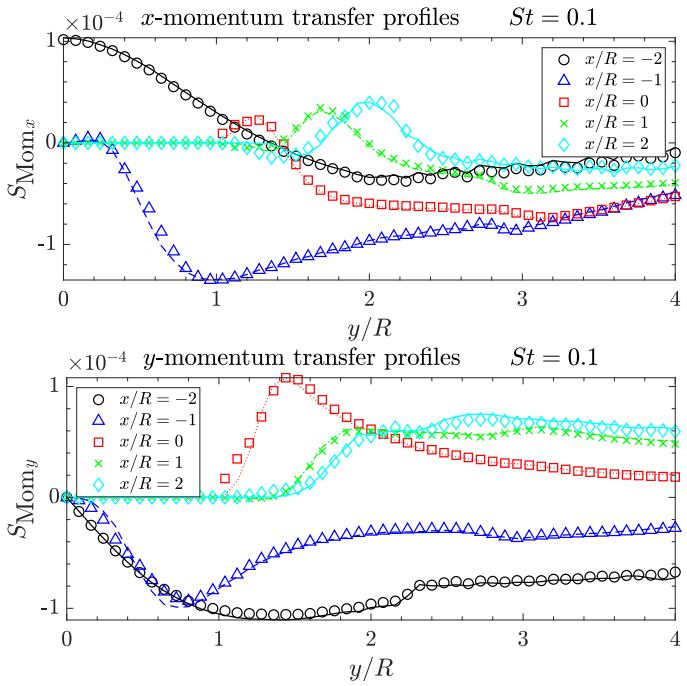

Figure 3. $x-$ and $y-$ momentum source term S_{Mom} profiles at selected cross-sections, FLA+kernel regression (symbols) vs CIC (curves), $Re = 20$, $St = 0.1$.

In the next step, the same approach was applied to a periodic flow with asymmetric vortex shedding, $Re = 100$. The results at $t = 50$, are shown in Figures 4 and 5. As can be seen, in the transient case the combined FLA and kernel regression approach returns results that are not smooth, and are sensitive to the mesh. The occurrence of spurious data increases as the flow develops at later simulation times, as it affects the carrier phase flow. Such behaviour may be attributed to the kernel regression procedure, where droplet parameter values are interpolated over a relatively large area, leading to significant values recorded in locations with no droplets.

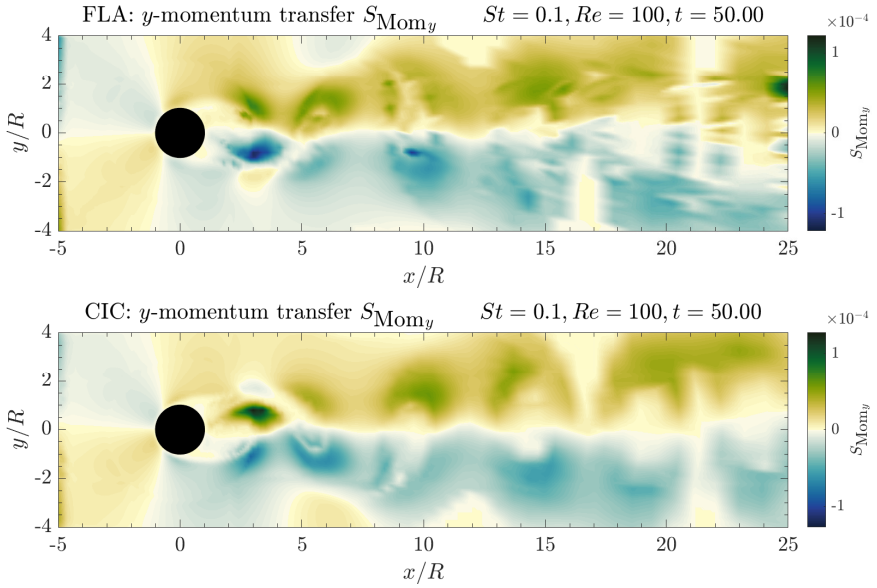

Figure 4. Distribution of the $y-$component of the momentum source term S_{Mom}, calculated using FLA + kernel regression (top) and CIC (bottom), $Re = 100$, $St = 0.1$, $t = 50$.

The final group of results is for droplet vapour transport. Again, we focus on the mass exchange term, which is presented in Figure 5. Both in steady-state and transient cases, the mass source term distribution is smooth.

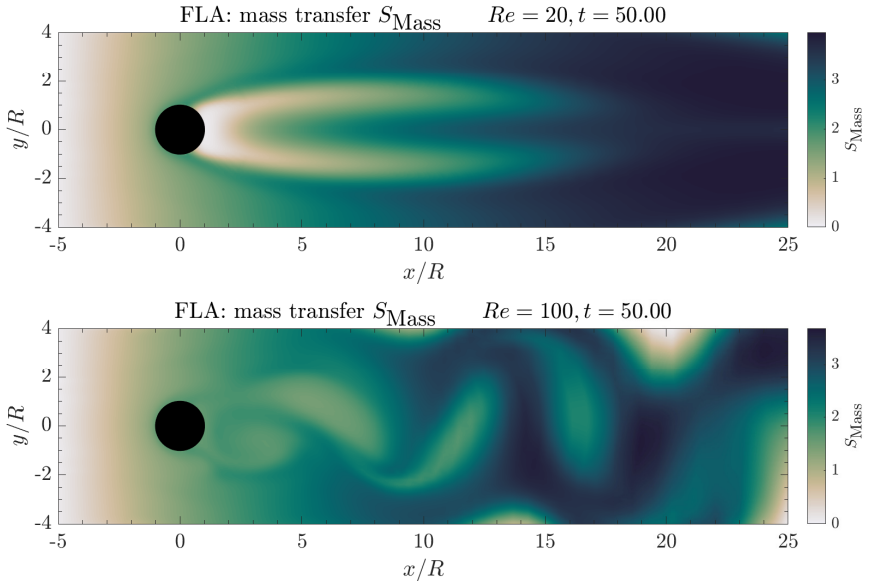

Figure 5. Distribution of the mass source term S_{Mass}, calculated using FLA + kernel regression, $Re = 20$ (top) and $Re = 100$ (bottom).

Conclusions

A two-way coupling approach, where the effect of droplets on the carrier phase flow is taken into account, has been implemented. In this approach the momentum and mass exchange source terms are calculated by combining the fully Lagrangian approach with kernel regression. This procedure has been implemented in OpenFOAM as an additional library.

Using kernel regression with the gFLA offers an efficient means of reconstructing the droplet probability density field for a smooth representation of interphase coupling source terms. The implementation of the approach has been examined versus the Cloud-in-Cell approach. It has been demonstrated that the results obtained using the new approach are in good agreement with the reference values in the case of steady state flow. However, for the case of transient flow, the momentum exchange source terms calculated using the combined FLA and kernel regression procedure exhibit some spurious behaviour, which needs to be investigated further. For the steady-state case, the results are obtained much faster, with a computational speedup factor of around 100 times being observed whilst obtaining the same level of fidelity and smoothness as the reference case.

Acknowledgements
The authors are grateful to the UKRI (Grant MR/T043326/1) for their financial support and to the University of Brighton for the access to the university's High Performance Computing Cluster.

Nomenclature

a	amplitude of the disturbance in equation (12)
c	droplet vapour concentration
D	diffusion coefficient [$m^2 \cdot s^{-1}$]
$\mathbf{f}$	force per unit mass [$N \cdot kg^{-1}$]
$\mathbf{H}$	bandwidth matrix [m^2]
h	smoothing length [m]
$\mathbf{I}$	identity matrix
$\mathbf{J}$	Jacobian tensor
k	wave number of the disturbance in equation (12)
K	kernel
l_{in}, l_{out}, l_w	computational domain dimensions
L	characteristic length scale [m]
m	mass of a particle/droplet [kg]
N	number of droplets that contribute at the point $\mathbf{x}$
n	spatial dimensionality of the problem (1D, 2D or 3D)
$n(\mathbf{x}, t)$	droplet number density
p	static pressure [Pa]
$p(\mathbf{x}, r, t)$	droplet probability density
r	droplet radius [m]
Re	Reynolds number
S_{Mass}	source term for mass exchange [$kg \cdot s^{-1}$]
S_{Mom}	source term for momentum exchange [$kg \cdot m \cdot s^{-1}$]
St_0	Reference Stokes number corresponding to the initial modal droplet size
t	time [s]
$\mathbf{u}$	gas velocity [$m \cdot s^{-1}$]
U	characteristic velocity scale [$m \cdot s^{-1}$]
$\mathbf{v}_d = (v_x, v_y, v_z)$	droplet velocity [$m \cdot s^{-1}$]
$\mathbf{x}_d = (x, y, z)$	droplet position [m]

Greek letters

δ	rate of change of the droplet surface area [$m^2 \cdot s^{-1}$]
μ	dynamic viscosity [Pa·s]
ρ	density [$kg \cdot m^{-3}$]
φ	rate of droplet radius change [$m \cdot s^{-1}$]
ζ	damping parameter in equation (12)

Subscripts

d	dispersed phase parameter along Lagrangian trajectories
i, j	component indices
0	initial value

Superscripts

i	droplet index
$\mathbf{x}$	index corresponding to the spatial variables
r	index corresponding to the droplet radius

Abbreviations

CIC	Cloud-In-Cell
FLA	fully Lagrangian approach
gFLA	generalised fully Lagrangian approach

References

[1] Sazhin, S. S., 2014, "Droplets and Sprays". Springer.
[2] Bourouiba, L., Dehandschoewercker, E., and Bush, J.W.M., 2014, *Journal of Fluid Mechanics*, 745, pp. 537–563.
[3] Dolovich, M.B. and Dhand, R., 2011, *The Lancet*, 377 (9770), pp. 1032–1045.
[4] Begg, S., Kaplanski, F. B., Sazhin, S. S., Hindle, M., and Heikal, M., 2009, *International Journal of Engine*

Research, 10 (4), pp. 195-214.
[5] Osiptsov, A.N., 2000, *Astrophysics and Space Science*, 274, 377.
[6] Healy, D.P., Young, J. B., 2005, *Proc the Royal Society A: Mathematical, Physical and Engineering Sciences*, 461, 2059, pp. 2197-2225.
[7] Li, Y., Rybdylova, O., 2021, *International Journal of Multiphase Flow* 142, 103716.
[8] Osiptsov, A. N., 1984, *Fluid Dynamics*, 19 (3), pp. 378–385.
[9] Stafford, C., Rybdylova, O., 2022, Sep. 6.-8. 2022, 31st European Conference on Liquid Atomization and Spray Systems.
[10] Hastie, T., Tibshirani, R., and Friedman, J.H., 2009, 'The elements of statistical learning: data mining, inference, and prediction'. Springer.
[11] Zdravkovich, M. M., 1997, 'Flow Around Circular Cylinders: A Comprehensive Guide Through Flow Phenomena, Experiments, Applications, Mathematical Models, and Computer Simulations'. Oxford University Press.
[12] Batchelor, G. K., 1999, 'An introduction to fluid dynamics'. Cambridge University Press.
[13] Laroussi, M., Djebbi, M., and Moussa, M., 2014, *Computers & Fluids*, 101, pp. 194–207.
[14] Bayraktar, E., Mierka, O., and Turek, S., 2012, *International Journal of Computational Science and Engineering*, 7 (3), p. 253.